Journal of Applied Fluid Mechanics, Vol. 16, No. 8, pp. 1531-1543, 2023.
Available online at www.jafmonline.net, ISSN 1735-3572, EISSN 1735-3645.
https://doi.org/10.47176/jafm.16.08.1635

Experimental Study on the Flow Pattern of Double-hemisphere Rough Elements with Different Streamwise Spacing

P. Chen, J. Sun†, Y. T. Cheng and W. Y. Chen

Department of Process Equipment and Control Engineering, Hebei University of Technology, Tianjin, 300130, China
National-Local Joint Engineering Laboratory for Energy Conservation in Chemical Process Integration and Resources Utilization, School of Chemical Engineering, Hebei University of Technology, Tianjin, 300130, China

†*Corresponding Author Email: sunjiao@hebut.edu.cn*

ABSTRACT

Particle image velocimetry is used to study the variation around single- and double-hemisphere rough elements with different streamwise spacings immersed in the boundary layer. Instantaneous velocity field information in the streamwise–normal and streamwise–spanwise directions is collected at a Reynolds number of 1800. 3R, 5R, and 7R are determined as the rough element spacing used in the double-hemisphere rough element experiment, representing the smaller, medium transition, and larger rough element spacing, respectively. The average velocity, Reynolds shear stress, shedding frequency, and proper orthogonal decomposition results of the flow field around the rough elements under various working conditions were compared. The downstream hemisphere will encroach on the streamline following the upstream hemisphere, and changing the spacing means changing the position of the encroached area. When the spacing is smaller, the streamline reattachment is destroyed, and the momentum and mass exchange between the two-hemisphere rough elements decreases. The double-hemisphere rough element is a slender, blunt, rough element. At the medium transition spacing, the shear layer and vortex structure shed from the upstream hemisphere are over the downstream hemisphere, and the double-hemisphere rough elements will cause disturbance in a larger wall-normal range. The streamline has been reattached at the larger streamwise spacing, and the interaction between the two hemispheres is the weakest. Here, the double-hemisphere rough element will form the recirculation zone, recirculation arch vortex, and periodic hairpin vortex.

Article History

Received October 30, 2022
Revised March 4, 2023
Accepted March 27, 2023
Available online May 31, 2023

Keywords:

Rough element
Streamwise spacing
Turbulence
PIV
Boundary layer

1. INTRODUCTION

Understanding the behavior of turbulent boundary layers is challenging in fluid mechanics. Engineered fluid mechanical systems include compressors, turbines, pumps, and reciprocating engines. These fluid mechanical devices have intricate wall constructions, including pits and uneven projections. Rough elements change the transition position of the boundary layer (Wassermann & Kloker, 2002). Rough walls typically increase drag; however, in some unique structures, such as microgrooves, the rough surface can also play a role in drag reduction (Yan et al., 2021; Zhang et al., 2021). Researchers frequently concentrate their research on regularly arranged geometric rough walls, such as hemispherical rough walls (Wu et al., 2020), because they are more conducive to controlling experimental research objectives. Although practical applications contain complex rough wall structures, they are more prototypical natural and artificial.

Due to its widespread use in fluid mechanical devices, the hemispherical rough element is a classic rough element with significant research significance. Jacobs (1938) conducted a pioneering analysis of a single-hemispheric rough element's near-wake and far-wake field. In studies on hemispherical rough element wake, many researchers have found structures similar to a hairpin vortices present in a smooth flat plate boundary layer (Klebanoff et al., 1961; Mochizuki, 1961; Cao & Tamura, 2020). A self-sustaining pattern causing the periodic shedding of hairpin vortices was discovered to exist behind large-scale hemispherical rough elements by Citro et al. (2015) after analyzing the generation and shedding process of hairpin-like packets within the Blasius boundary layer.

Acarlar and Smith (1987) used hot-film anemometry, hydrogen bubbles, and dye injection to qualitatively and

Nomenclature

R	hemisphere rough element radius	x	streamwise direction
U_∞	free-flow velocity	y	normal height direction
u	local streamwise velocity	z	spanwise direction
v	local wall-normal velocity	L	streamwise spacing
w	local spanwise velocity		

quantitatively determine the vortical structure produced by hemispheres. Extensive measurements were carried out in the Reynolds number ($Re_R = RU/\upsilon$) range $120 < Re_R < 3400$ to study quasi-periodic hairpin vortices shed from the hemisphere. It was discovered that the vortex formation depended critically on the low pressure area in the near-wake of the hemisphere. Once the boundary layer separates from the hemisphere, the area of low pressure pulls the fluid downstream. The external irrotational flow field begins to bend inward, resulting in a narrowing of the region between the separated shear layer and the wall. The centrifugal force field formed by the inward-spiraling motion of the outer flow causes the vortex lines to concentrate, forming a hairpin vortex. In addition, they discovered that the upstream stagnation point of the hemisphere generated a horseshoe-shaped standing vortex. Savory and Toy (1986) also found a similar horseshoe-shaped vortex structure, while they found a shedding vortex structure with periodic interaction with the shear layer in the near-wake field of an isolated hemispherical rough element wake, which is very similar to the hairpin vortex described by Acarlar and Smith. They later derived a schematic structure of the shear layer in the wake of an isolated hemispherical rough element from the distribution of turbulent shear stress and mean velocity (Savory & Toy, 1988). Carr and Plesniak (2016) named the hairpin vortex discovered by Acarlar and Smith as the Shear Layer Hairpin vortex and defined the recirculation arch (RA) vortex formed by shear layer coiling.

In the research by Waigh and Kind (1998), it is proposed to determine whether the rough wall is sparse or compact using the geometric size of the rough element arrangement, including rough element size, spacing parameters, and so on. Based on this method, 3R, 5R, and 7R are determined as the rough element spacing used in the experiment, representing the smaller rough element spacing, the medium transition rough element spacing and the larger rough element spacing, respectively. The research of Waigh and Kind suggests that the rough element spacing is an important parameter affecting the turbulent boundary layer of a rough wall surface. Therefore, it is important to explore the effect of double-hemisphere rough element spacing on the fine structure in the surrounding flow field, which is of great significance for controlling the turbulent boundary layer by using hemispherical rough wall.

There are many related studies on the influence of rough element spacing on boundary layer flow (Spivack, 1946; Le et al., 1990, Sumner et al., 1999). In an experimental study by Zhou et al. (2006) on the wake of two-tandem-cylinder, it was found that the flow behind two-tandem-cylinder was typically divided into three states depending on whether the shear layer separated from the upstream cylinder impacted or reattached to the downstream cylinder before forming a vortex street, or formed a vortex between the cylinders. Kim et al. (2019) arranged two identical finite-length cylinders in tandem and fully submerged in the boundary layer of a turbulent channel flow and found strong interactions between the shear layers separated from each cylinder. Hamed et al. (2019) performed particle image velocimetry (PIV) experiments on two vertical cylinders with varying streamwise direction spacing. They found that the upstream cylinder would cause a downward shift and size reduction in the recirculation zone of the downstream cylinder, and that when the streamwise direction spacing is low enough, the recirculation zone behind the upstream cylinder recirculation zone will attach to the downstream cylinder. Liu et al. (2022) studied the three-dimensional characteristics of the flow field around double-cone with different streamwise direction spacings and classified the flow structure between double cones with varying spacing into three states: shear layer wrapping state, transition state, and wake impingement state.

Accord to existing research, the study of rough element spacing in multiple discrete rough elements is mainly focused on multiple cylindrical rough elements with different spanwise and streamwise spacing, while few studies on the streamwise spacing of hemispherical rough elements. Only Barman et al. (2016) conducted experiments on double-hemisphere rough elements with multiple streamwise spacing arranged in series interacting with a combined wave flow, which focused on the changes in turbulence statistics caused by the superposition of surface waves of different frequencies on the background flow, while the analysis of the rough element spacing was relatively plain. Dai et al. (2012) also performed direct numerical simulation experiments under similar conditions, which also focused only on the variation in turbulence statistics.

In this study, PIV was used to study the flow field around a single-hemisphere and double-hemisphere rough elements with three representative-sized streamwise spacing to investigate, and the effects of the streamwise direction spacing on the mean velocity, turbulence intensity, periodic hairpin vortex, and RA vortex in the rough element wake were investigated.

2. EXPERIMENTAL SETUP

The total length of the experimental water channel was 7.5 m, mainly including the rectification section, contraction section, test section, power section, and reflux section. The rectification section is equipped with a honeycomb and damping net, which can rectify and eliminate the large-scale water flow structure. The contraction section is designed according to the

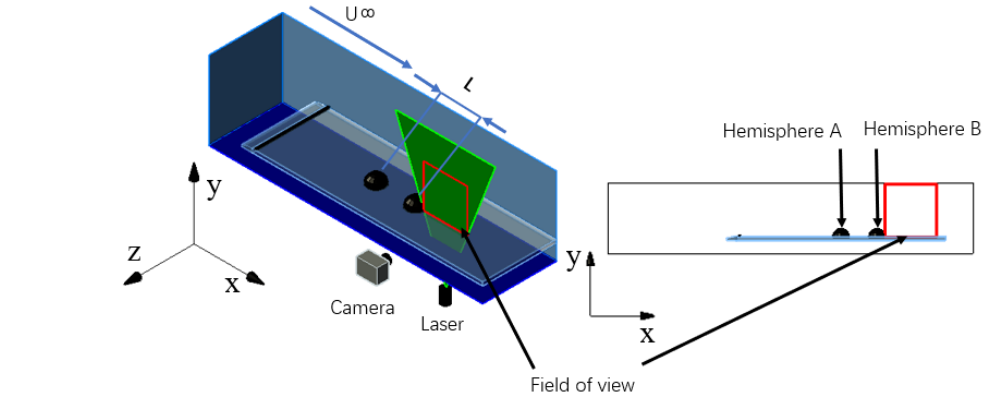

(a)

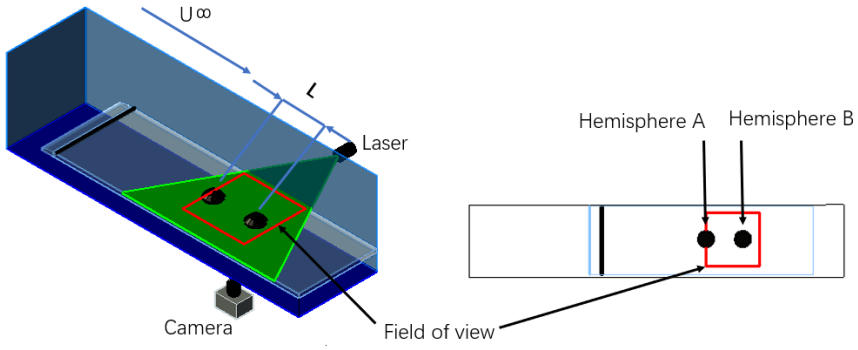

(b)

Fig. 1. Schematic diagram of the experimental setup and shooting: (a) streamwise–normal (x–y) plane flow field. (b) streamwise–spanwise (x–z) plane flow field.

contraction curve to reduce the flow separation in the rectification section. A smooth plexiglass plate with 8:1 elliptical modification at the leading edge and 2200 mm × 500 mm × 20 mm (length × width × thickness) was horizontally placed in the test section, which is 2500 × 500 × 600mm^3. This method was verified in the experiment by Gao et al. (2021), and the background turbulence in the experimental section can be less than 0.8%.

In the experiment, the flow is controlled to be fully developed turbulence by a tripwire. A fully developed turbulent boundary layer is obtained by a 5-mm-diameter spanwise turbulence line located 100 mm downstream of the elliptical leading edge of the flat plate, and the pressure gradient of the flow is close to zero by adjusting the trailing edge height of the flat plate. Hemisphere B with a radius of 10 mm is set 1400 mm from the plate's front edge and 250 mm from the wall surface, and hemisphere A of the same size is set at an upstream distance L to form a double-hemisphere rough element structure, where L is the spacing between the two hemispheres. According to Waigh's method (1998), we decided to use spacing L of 3R, 5R, and 7R between the two hemispheres. In this experiment, the streamwise hemisphere rough element spacing L is taken as 3R, 5R, and 7R, representing smaller rough element spacing, medium transition rough element spacing and larger rough element spacing. The streamwise, wall-normal, and spanwise coordinates are denoted as x, y, and z, respectively, and the corresponding velocity components are denoted as u, v, and w. The origin of the coordinates is located at the trailing edge of the downstream hemisphere B, where it meets the wall.

The free-flow velocity is adjusted to U∞ = 0.18 m/s, and the experimental temperature is 20 °C. The density of water is ρ_f = 998 kg/m^3, and the kinematic viscosity (υ) of water is υ = 1.006 mm^2/s. Polystyrene particles with area-averaged diameters of 20 μm were selected as tracer particles to track the liquid phase. After adding the hemispherical rough elements, Re_R is 1800 ($Re_R = RU/\nu$, R = 10 mm) and the top of the rough element is located at $y^+ = 78$, which is in the log-law region.

The PIV system from LaVision, Germany, was used for data acquisition. The laser model was LPY 700, a double-pulse laser with a maximum frequency of 100 Hz and a maximum energy of 100 mJ, emits a green light source at a wavelength of 532 nm. The camera was a 4MX camera (2048 × 2048 pixels2), and the maximum sampling frequency was 180 Hz. Double frame and double exposure were used to image acquisition at 90 Hz, and the exposure time meets the displacement of more than 5 pixels between the two frames. The number of particle images per pixel is 0.01. The collection of flow field information in this experiment was divided into two parts: streamwise–normal (x–y) plane flow field and streamwise–spanwise (x–z) plane flow field. Among them, the wake flow field of the two hemispheric asperity elements is collected on the x-y plane and the flow field at the normal height of y = 0.9R is presented on the x-z plane. The measurement scheme is shown in Fig. 1.

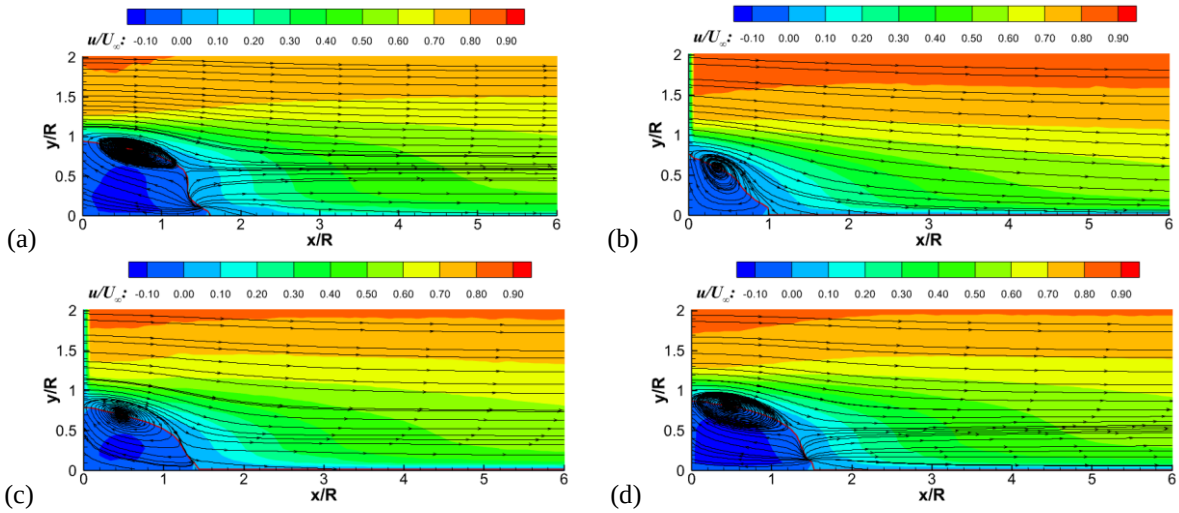

Fig. 2. Average velocity field of rough element wake: (a) Single-hemisphere rough element. (b) Double-hemisphere rough element with L = 3R. (c) Double-hemisphere rough element with L= = 5R. (d) Double-hemisphere rough element with L = 7R.

12000 pairs of images were collected under every condition with an actual image size of 105 mm × 105 mm, which means 1 pixel = 0.0512 mm.

The cross-correlation algorithm is used for data processing, and the interrogation window is 32 × 32 pixels2 with 50% overlap to obtain 128 × 128 velocity vectors. The selection of interrogation window size and overlapping can ensure that the particles are displaced by 5 to 8 pixels between the two frames, which meet the one-quarter rule. The space interval between the vectors was 0.834 mm.

3. TURBULENCE STATISTICS

To analyze the regulation effect of different spacing between double-hemisphere rough element structures arranged streamwise at the boundary of fully developed turbulence, both the streamwise–normal velocity field passing through the center of the hemispheres and the streamwise–spanwise velocity field at a wall-normal height of 0.9R are post-processed.

3.1 Average Velocity

Figure 2 shows the time-averaged streamwise velocity contours in the wake of single-hemispherical and double-hemisphere rough elements with different streamwise spacing, reflecting the average flow pattern of the rough element wake. The intersection of the wall with zero mean flow velocity contour boundary is the reattachment position of the streamlines.

The recirculation zone is found to be slightly reduced in double-hemisphere rough element wake compared to the single-hemisphere wake, and as the streamwise rough element spacing L increases, the size of the recirculation zone becomes larger. There is a large-scale vortex structure above the recirculation zone, which also gradually increases with the increase in the L value. This is because in double-hemisphere rough element wake, the fluid crossing the downstream hemisphere B is slowed down by the upstream hemisphere A and has a lower velocity than the single-hemisphere rough element. Increasing the spacing between rough elements enhances the recovery of fluid velocity. The formation of the recirculation zone and the large-scale vortex structure are related to the magnitude of the velocity gradient of the fluid crossing the rough element relative to the fluid in the recirculation zone. Therefore, the extent of the recirculation zone and the strength of the large-scale vortex structure are reduced with an L increase in the double-hemisphere rough element.

For the roughness element spacing of L=7R, the double-hemisphere wake exhibits the strongest large-scale vortex structures and the most dense vortex lines. This is because at larger spacing, the fluid velocity downstream of hemisphere A has already recovered to a larger value, which enlarges the recirculation zone of the double-hemisphere roughness elements and leads to the strongest recirculation zone. This is similar to the flow characteristics of two cylindrical roughness elements at the same height, fully immersed in a developing channel flow studied by Kim and Christensen (2018). With the increase of the spacing between roughness elements, the range of the downstream reattachment zone expands, and the range and intensity of large-scale vortex flow increase.

To further distinguish the stereoscopic influence of streamwise rough element spacing on the flow characteristics in the wake region of the single-hemisphere rough and double-hemisphere rough elements, the time-averaged streamwise velocity contour on the streamwise–spanwise plane at the wall-normal height y = 0.9R near the top of the hemisphere is shown in Fig. 3. Although shadows appear on the backside of the photographed region due to the unidirectional horizontal laser, this does not affect the resolution of double-hemisphere rough element wake structure of experimental interest.

On the plane of y = 0.9R, unlike the wake of double-hemisphere rough element with L = 3R, a reflux structure appears downstream of hemisphere A in the double-hemisphere rough element at L = 5R and L = 7R. This is because the obstructive effect of hemisphere B on the

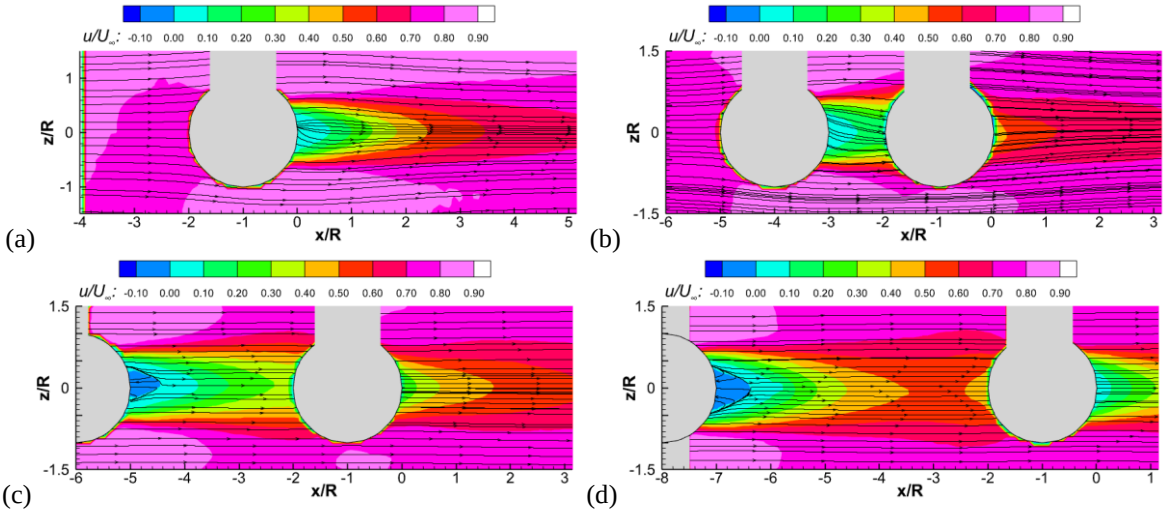

Fig. 3. Average velocity field of streamwise–spanwise plane flow field around rough element: (a) Single-hemisphere rough element. (b) Double-hemisphere rough element with L = 3R. (c) Double-hemisphere rough element with L = 5R. (d) Double-hemisphere rough element with L = 7R.

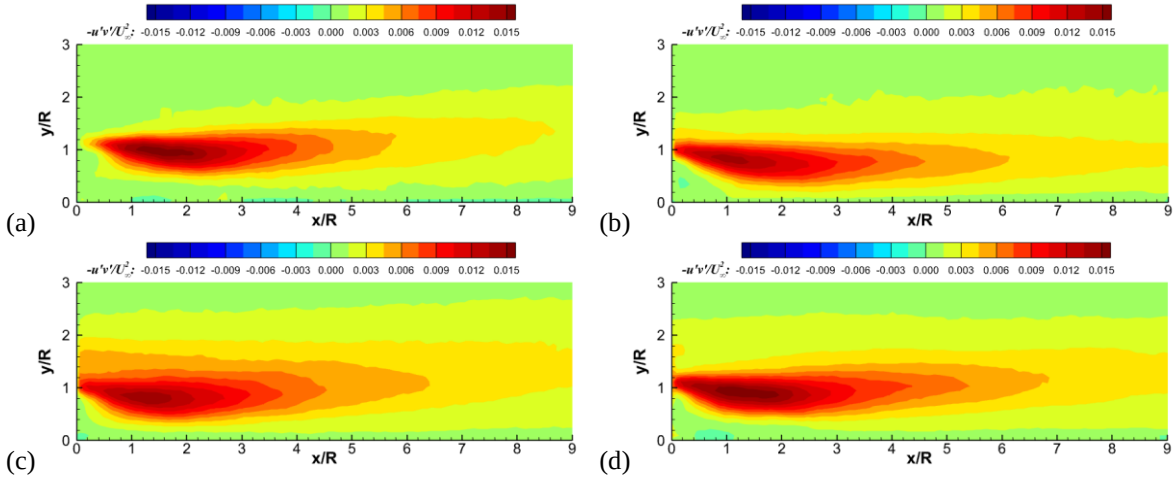

Fig. 4. Reynolds shear stress nephogram of rough element wake: (a) Single-hemisphere rough element. (b) Double-hemisphere rough element with L = 3R. (c) Double-hemisphere rough element with L = 5R. (d) Double-hemisphere rough element with L = 7R.

upstream fluid causes the velocity of the fluid between hemisphere A and hemisphere B to decrease, resulting in a larger velocity gradient at the recirculation zone of hemisphere A, which leads to an increase in the size of the recirculation zone. At L = 3R, the absence of the reflux structure downstream of hemisphere A is due to the recirculation region of hemisphere A is encroached upon by the downstream hemisphere B when the spacing is close enough. Smaller streamwise spacing leads to closed streamlines between the double-hemisphere roughness elements and a significant reduction in momentum and mass exchange with the external flow field. This means that the entire structure composed of the double-hemisphere roughness elements and their internal flow can be approximated as a bluff body roughness element.

3.2 Reynolds Shear Stress

Figure 4 shows the Reynolds shear stress cloud diagram of the rough element wake, the physical meaning of which is the additional stress generated in the momentum exchange process caused by velocity pulsation, which represents the strength of turbulent flow transport. The Reynolds shear stress in the wake of double-hemisphere rough element is found to increase significantly over a larger range of wall-normal compared to the single-hemisphere rough element. The Reynolds shear stress in the wake of double-hemisphere rough element gradually increases with increasing streamwise spacing and reaches a maximum at L = 7R, when the Reynolds shear stress distribution in the wake of double-hemisphere rough element is most similar to that of the single-hemisphere.

It is also found that the region where the Reynolds shear stress in the near-wall region tends to be close to zero increases with increasing rough element spacing. This indicates that the influence of the shear layer and vortex structure induced by double-hemisphere rough element on the flow field near the wall is gradually weakened, and the momentum exchange becomes more concentrated. The

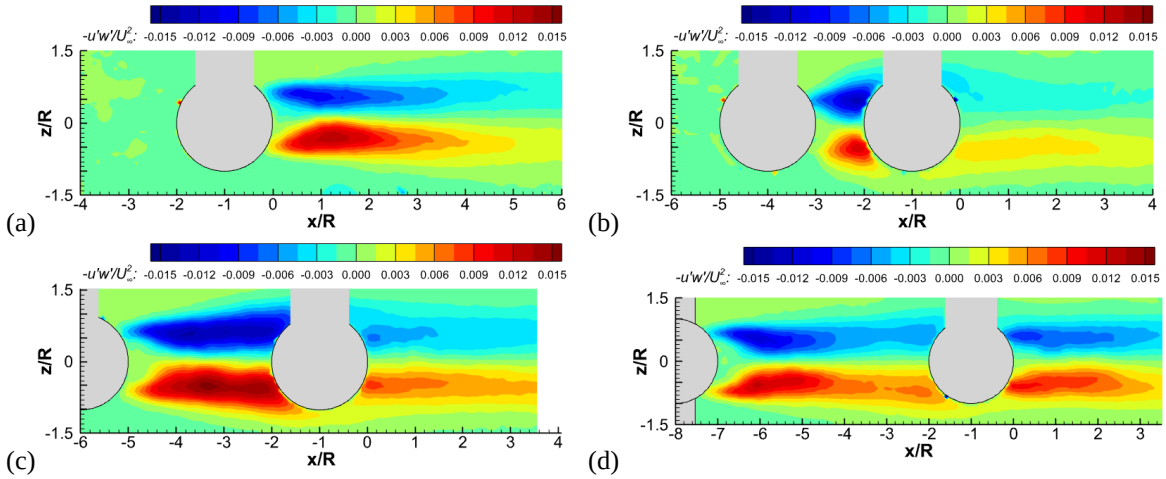

Fig. 5. Reynolds shear stress nephogram of streamwise–spanwise plane flow field around rough element: (a) Single-hemisphere rough element. (b) Double-hemisphere rough element with L = 3R. (c) Double-hemisphere rough element with L = 5R. (d) Double-hemisphere rough element with L = 7R.

shear layer and vortex structure caused by double-hemisphere rough element are further away from the wall, and the degree of momentum exchange with the main flow is relatively higher.

Figure 5 provides the Reynolds shear stress contour in the wake region of the flow spread (x-z) of double-hemisphere rough element at a wall-normal height of y = 0.9R on the streamwise–spanwise plane. It can be clearly seen that the Reynolds shear stress is mainly present in the flow field between two hemispheres at L = 3R, showing a symmetrical attitude, while in the downstream wake of double-hemisphere rough element, the Reynolds shear stress at this normal height causes little effect. At L = 5R, the Reynolds shear stress is also symmetrical in the region of the flow field between the two hemispheres and fills the entire interval, while in the downstream wake of double-hemispherical rough element, the Reynolds shear stress is significantly reduced, but is still symmetrical. With the increase of the streamwise spacing, the Reynolds shear stresses in the wake of both hemispherical rough elements appear symmetrically at L = 7R, and the Reynolds shear stresses in the wake of the upstream hemisphere are stronger than those in the downstream hemisphere.

The difference in the Reynolds shear stress structure in the flow field around the double-hemisphere rough element with different streamwise spacing is due to the Reynolds shear stress region in the wake of the upstream hemisphere is occupied to varying degrees by the downstream hemisphere. The region where the Reynolds stresses are located is mostly occupied by the downstream hemisphere at L = 3R, the back-end region is occupied at the medium spacing L = 5R, and there is no significant encroachment at L = 7R, due to the downstream hemisphere being farther away from the high stress region in the upstream hemisphere wake. It can be seen that the position of the downstream hemisphere in the wake of the upstream hemisphere determines the magnitude and influence range of Reynolds shear stress, which is also the main reason for the difference in macroscopic statistics of the double-hemisphere rough element wake at different rough element spacing.

3.3 Turbulence Intensity

Figure 6 shows the turbulence intensity cloud in the range of {x = (0-9) R, y = (0-3)R} after the rough element, which is calculated as follows:

$$Tur = \frac{\sqrt{(\overline{u'^2}+\overline{v'^2})}}{U_\infty} \quad (1)$$

The presented study investigates the turbulence intensity characteristics of the wake behind a double-hemisphere roughness element, as shown in Fig. 6. The study reveals that the turbulence intensity of the wake increases progressively with an increase in the streamwise spacing L between the roughness elements. This increment is accompanied by an increase in the streamwise spacing L, resulting in a gradual rise in the turbulence intensity within the recirculation region of hemisphere B. Notably, the maximum disturbance within the wake of the double-hemisphere roughness element is observed when L=7R.

Upon introducing the upstream hemisphere A, the downstream turbulence intensity of hemisphere B increases significantly in the normal direction, particularly within the range of y = (1-1.8) R at L = 5R. This is because the shear layer separated from hemisphere B and the induced vortex structures are not obstructed by hemisphere B as in the larger spacing L=7R or merged with the shear layer separated from hemisphere B as in the smaller spacing L=3R. Instead, they cross over hemisphere B from above and interact with the separated shear layer from hemisphere B, resulting in a higher turbulence intensity at the normal height range of y = (1-1.8) R in the wake of double-hemisphere rough element.

3.4 Shedding Frequency

In studies of single-hemispherical rough element streaming, many scholars have identified shedding of

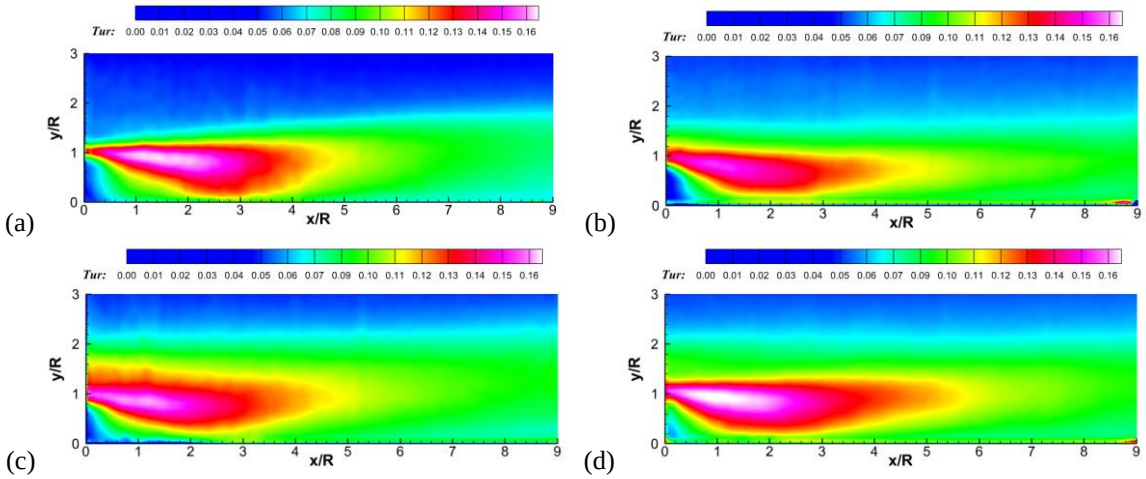

Fig. 6. Turbulence intensity nephogram of rough element wake: (a) Single-hemisphere rough element. (b) Double-hemisphere rough element with L = 3R. (c) Double-hemisphere rough element with L = 5R. (d) Double-hemisphere rough element with L = 7R.

quasi-periodic wake structures downstream of hemispherical rough elements (Savory & Toy, 1986; Acarlar & Smith, 1987; Savory & Toy, 1988; Carr & Plesniak, 2016; Zhang et al., 2020; Gao et al., 2021). The relationship between power energy and frequency of the shedding vortex time series signal was analyzed using power spectral density (PSD), and the periodicity of the shedding of wake vortices was explored in order to ascertain whether such quasi-periodicity exists downstream of double-hemispheres and to further investigate its regularity. In this paper, the wall-normal pulsation velocity is used as the original signal, and the Welch method is used to estimate the PSD at x = 1R, 2R, 6R for double-hemisphere rough element wake.

Figure 7 shows the PSD plots of shedding frequency in the wake of single-hemisphere rough element or double-hemisphere rough elements with different flow spacing. A periodic structure with a frequency of 2.29 Hz is found to occur within x = (2-6) R in the single-hemisphere wake; moreover, this frequency becomes dominant after x > 3R and it should be the frequency corresponding to the periodic hairpin vortex. In the double-hemisphere rough element wake, structures with multiple scales are always present, most of which with small amplitudes, and they should be small-scale structures caused by complex rough elements flowing around. For structures with large amplitudes, there are two main frequencies at L = 3R, 1.98 Hz and 0.37 Hz, the former occurring mainly within x = (2-4)R and the latter mainly at x = 5R and downstream. The change of main frequency in x=(1-3)R in Figure 7b corresponds to the hairpin vortex generated when the two-hemisphere rough element approximates to a blunt body with a short rough element interval. This hairpin vortex falling off the slender bluff body is unstable and will decay quickly, resulting in a reduction in the corresponding main frequency. In L = 5R, the two main frequencies are 2.40 Hz and 2.30 Hz, the former occurring mainly within x = (1-4)R and the latter mainly at occurring in x = 5R and downstream of it. In L = 7R, the main frequency is 2.94 Hz, which starts to occur at x = 3R.

According to the theory of Acarlar and Smith (1987), a detached shear layer from a single-hemispherical rough element induces a periodic hairpin vortex structure at downstream, which explains the main frequency in a single-hemispherical rough element starting at x = 2R. The main shedding frequency in the range x = (3-4)R was made dimensionless, using the dimensionless number Strouhal number S based on hemispherical radius, free-flow velocity, and shedding frequency, which was calculated as follows:

$$S = \frac{Rf}{U_\infty} \tag{2}$$

Here, R is the radius of the hemisphere and f is the main shedding frequency. Table 1 shows a table of S values corresponding to f values for each operating condition. Zdravkovich (1987) and Xu & Zhou (2004) both found that at larger rough element flow spacing, after the vortex dislodged from the upstream cylinder strikes the downstream cylinder, the upstream rough element and the downstream rough element simultaneously shed the vortex structure with similar frequency. Xu & Zhou (2004) found that the S-value varies with the size of the spacing; at smaller spacing, the shear layer separated by the upstream the cylinder is rolled up behind the downstream cylinder to form a vortex street. As the spacing increases, the shear layer separated from the upstream rough element is then attached to the downstream rough element, and as the spacing increases further, both rough elements shed vortices at the same time and the S value rises slowly until it approaches a constant.

In Table 1, we find that the S value gradually increases from 0.110 to 0.163 as the rough element spacing increases, which is basically consistent with the experimental conclusions of Xu & Zhou (2004). The analysis of the Reynolds shear stress contour in the direction of the integrated flow spreading shows that at the

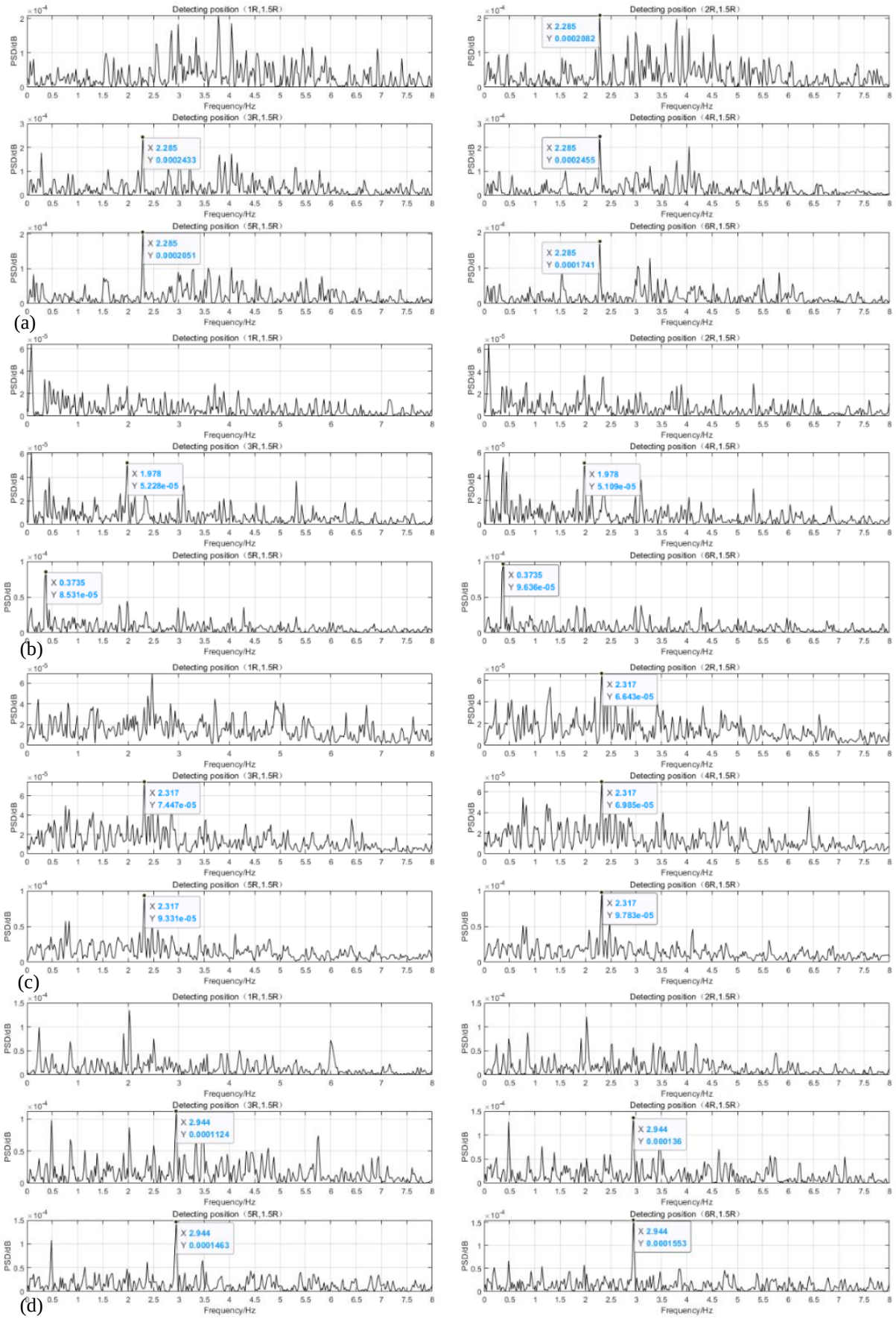

Fig. 7. Power spectral density diagram of rough element wake: (a) Single-hemisphere rough element; (b) Double-hemisphere rough element with L = 3R; (c) Double-hemisphere rough element with L = 5R; (d) Double-hemisphere rough element with L = 7R.

Table 1 S value and f value of each operating condition

Rough element spacing L	*S*	*f*/hz
Single-hemisphere	0.127	2.29
L=3R	0.110	1.98
L=5R	0.129	2.32
L=7R	0.163	2.94

smaller spacing L = 3R, the shear layer separated from the upstream hemisphere covers the downstream hemisphere and forms a vortex street downstream. At L = 5R, the shear layer separated from the upstream hemisphere then attached to the downstream hemisphere. At L = 7R the downstream wake of double-hemisphere rough element and the vortex street shedding between the two rough elements both appear, when the interaction between the two hemispheres is weakest.

4. PROPER ORTHOGONAL DECOMPOSITION

4.1 Proper Orthogonal Decomposition Method

Proper orthogonal decomposition (POD) is an effective method to extract coherent structure in a turbulent flow field. It was first introduced into fluid mechanics by Lumley (1967).

In classical POD calculations, two-dimensional (2D) velocity field information can be decomposed into:

$$x(\xi, t_i) = \sum_{j=1}^{n} a_j(t)\Phi_j(\xi) \tag{3}$$

Here, Φ_j is the eigenmode of the j^{th} mode, also known as the basis function, $a_j(t)$ is the modal time coefficient representing the time dynamics, and n is the total number of modes in the set (Deng et al. 2018).

The POD method can project high-order and nonlinear systems into a low-dimensional state space through orthogonal modes, ensuring the minimum residual error for a specified number of modes (Noack, 2016). The number of modes required to be able to represent the flow field data in an optimal manner and with a minimum number is determined by solving for the eigenvector Φ_j and the eigenvalue λ_j. The eigenvalues and eigenvectors are obtained by equation (4):

$$R\Phi_j = \lambda_j\Phi_j, \Phi_j \in \mathbb{R}^n,\ \lambda_1 \geq \cdots \geq \lambda_n \geq 0 \tag{4}$$

Here, R is the covariance matrix of the vector $x(t)$, which describes the time correlation of the flow field at two moments, and the eigenvalues λ usually only keeps r modes:

$$\sum_{j=1}^{r}\lambda_j \Big/ \sum_{j=1}^{n}\lambda_j \approx 1 \tag{5}$$

However, when the spatial size n of the data is large, the spatial scale $(n \times n)$ of the correlation matrix with the size $R = XX^T$ is large, making it nearly impossible to find the feature function using the classical spatial POD method.

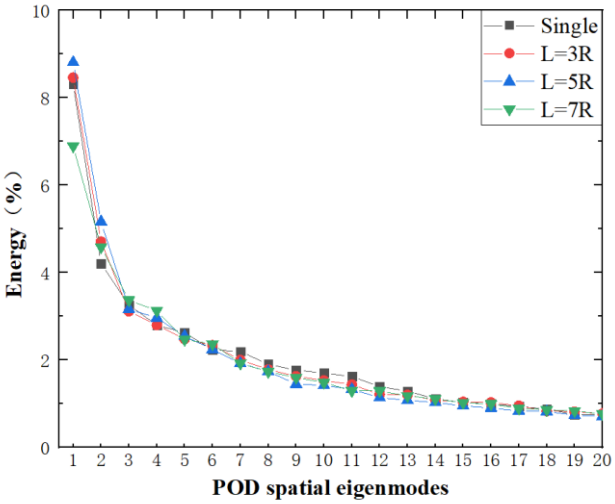

Fig. 8. Energy share of the first 20 orders of POD results

In snapshot POD technology, $x(t_i)$ is collected from snapshots taken at discrete times t_i, i =1, 2, …, m, where $m \ll n$, to solve a smaller scale $(m \times m)$ eigenvalue problem for the POD modes, significantly reducing the required computing and storage resources (Sirovich, 1987). In snapshot POD technology, the matrix R is obtained by equation (6):

$$R = \sum_{i=1}^{m} x(t_i)x^T(t_i) = XX^T \in \mathbb{R}^{n\times n} \tag{6}$$

In this study, the streamwise–normal two-dimensional velocity field obtained by PIV measurement is decomposed into modes with different scales by POD, and the contribution of each mode to the energy is evaluated. Therefore, each spatial mode represents a basic flow structure from an energy point of view.

4.2 POD Results

Using snapshot POD technology to extract main wake structures of single-hemisphere and double-hemisphere. Calculating with 6000 snapshots is sufficient to obtain converged POD results. The ratio of the first 20 POD modes to the total energy of the flow field is shown in Fig. 8.

Figure 9 shows the POD modes in which a periodic hairpin vortex starts to appear in the POD results, and the streamwise and wall-normal components of each mode are given. The periodic hairpin vortex obtained in POD results is similar to the behavior of the periodic structures obtained by Acarlar and Smith (1987) using flow display separation. However, because the wall turbulence used in the experiments is fully developed, the fluid will be generating coherent structures on the wall (Dong et al., 2020), which may cause the order of periodic hairpin vortex to appear relatively later.

The comparison shows that in the single-hemisphere, the periodic hairpin vortex structure appears in the 4th mode with an energy fraction of about 2.8%. With the addition of upstream hemisphere A, the periodic hairpin vortex structure in the hemisphere B wake becomes larger

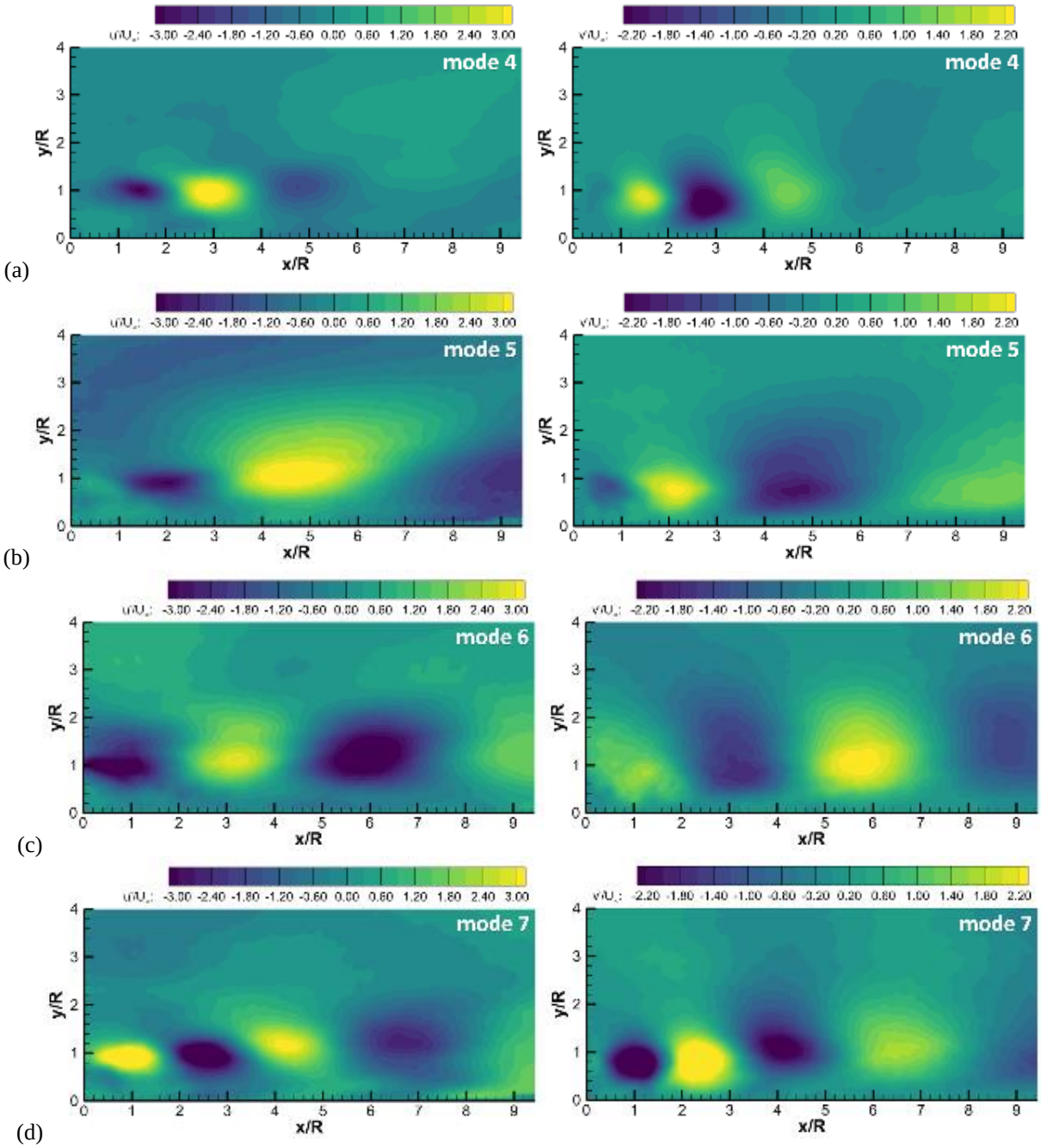

Fig. 9. Corresponding modes of periodic hairpin vortex in the POD results: (a) Single-hemisphere rough element; (b) Double-hemisphere rough element with L = 3R; (c) Double-hemisphere rough element with L = 5R; (d) Double-hemisphere rough element with L = 7R.

in scale, with a slight increase in vortex spacing and vortex intensity. This periodic hairpin vortex structure occurs in the 5th mode with an energy fraction of about 2.4% at L = 3R, in the 6th mode with an energy fraction of about 1.9% at L = 5R, and in 7th mode with an energy fraction of about 2% at L = 7R. The periodic hairpin vortex induced in L = 3R grows rapidly in the near-wake region (x < 1R) and begins to dissipate in the middle- and far-wake (after x > 6R).

This may be because the double-hemisphere with L = 3R can be approximated as a monolithic blunt body double-hemisphere rough element and the wake has a larger fluid flow velocity near the y = 0.9R wall-normal height plane, resulting in an unstable structure of its induced periodic vortices. Although the same hairpin vortex-like structure is found at L = 5R, the interaction of the periodic vortex structure induced by hemisphere A with the shear layer separated by hemisphere B results in this structure being further away from the wall and the vortex structure being more extensive and widely spaced. At L = 7R, the periodic hairpin vortices behave similarly to those in the single-hemisphere, but they are present in the streamwise direction to a much greater extent in the double-hemisphere rough element wake than in the single-hemisphere rough element wake with the same orientation.

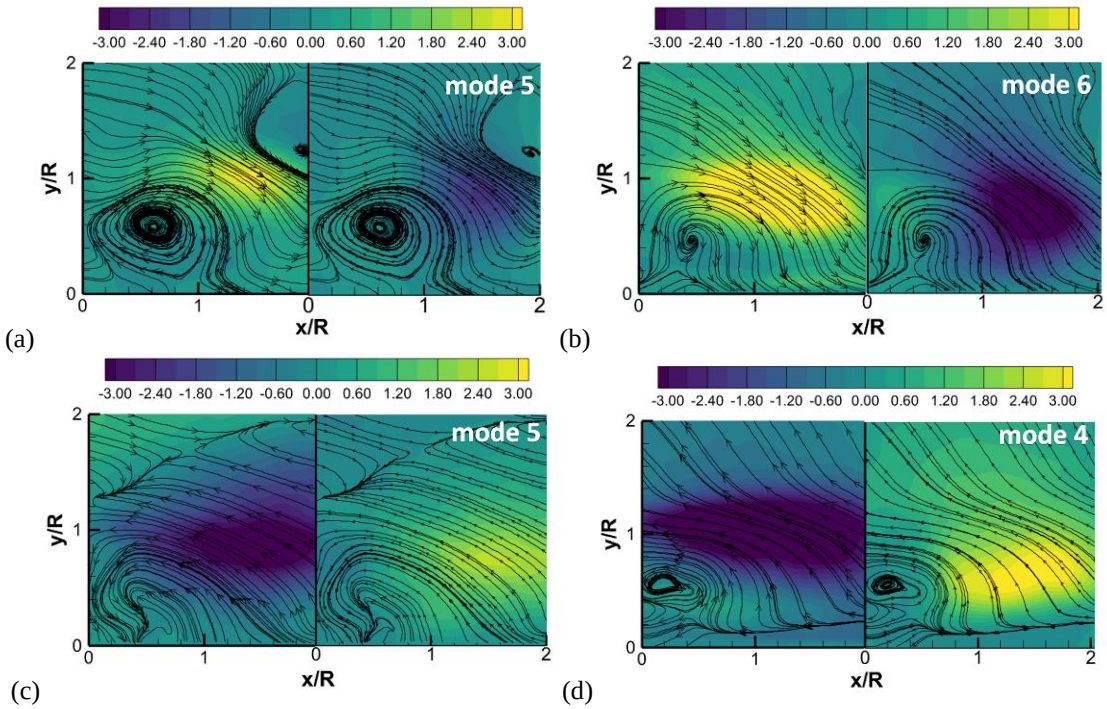

Fig. 10. Corresponding modes of the RA vortex in the POD results: (a) Single-hemisphere rough element; (b) Double-hemisphere rough element with L = 3R; (c) Double-hemisphere rough element with L = 5R; (d) Double-hemisphere rough element with L = 7R.

This suggests that the presence of hemisphere A, which is farther from hemisphere B, has a significant contribution to the enhancement of the periodic vortex, leading to the rough element bypass flow being influenced by the periodic vortex in the distant trails as well.

Figure 10 shows the POD mode where the steady-state RA vortex is located the RA vortex, first proposed by Carr and Plesniak (2016), is formed by the shear layer coiling up downstream of the hemisphere and dominates the formation of the reflux zone. The large-scale structure in the reflux zone is the result of averaging the RA vortex in the time dimension. RA vortices occur in the 5th mode with an energy fraction of ~2.6% in a single-hemispheric rough meta-trace, in 6th mode with an energy fraction of ~2.3% in L = 3R, in the 5th mode with an energy fraction of ~2.5% in L = 5R, and in the 4th mode with an energy fraction of ~3.1% in L = 7R. The energy share of the RA vortex is found to increase with increasing flow spacing and reaches a maximum in L = 7R, which is consistent with the previous conclusion that increasing flow spacing promotes an increase in the scale and intensity of the recirculation zone.

5. CONCLUSION

Obstacle arrangement plays an important role in the regulation of the flow around double-hemisphere rough element, and it is important to investigate the characteristics of the flow structure around a double-hemisphere rough element with different spacing to control the turbulent boundary layer using a hemisphere rough wall. In this paper, we used PIV to measure the instantaneous velocity field information of the flow field around a single-hemisphere and a double-hemispherical rough element with different flow spacing in the wall turbulent boundary layer of Re_R 1800, comparing and analyzing the mean velocity field and Reynolds shear stress in the surrounding flow field, track the shedding frequency of the periodic vortex structure in the wake using PSD, and analyze the effect of different flow spacing on the flow structure of double-hemispherical . The effect of different flow spacing on the periodic flow structure and RA vortex of the rough element wake was analyzed from an energy perspective by POD, and the following conclusions were obtained.

(1) At small flow spacing (e.g., L = 3R), double-hemisphere rough element can be approximated as an elongated blunt rough element due to the reduced momentum and mass exchange between the two hemispheres.

(2) At medium transition flow spacing (e.g., L = 5R), there is a stronger Reynolds shear stress between the two hemispheres in the spreading direction due to the encroachment of the downstream hemisphere into the strong Reynolds shear region in the wake of the upstream hemisphere. The two-hemisphere rough elements at this spacing are strongly perturbed in the larger wall-normal range.

(3) In double-hemisphere rough element wake, the strength and scale of the return zone increase with increasing flow direction spacing, and at larger flow direction spacing (e.g., L = 7R), double-hemisphere rough element promotes the formation of RA vortices, resulting in a return zone of greater scale

and strength than the single-hemisphere rough element winding condition.

(4) The downstream hemisphere will encroach on the streamlines in the upstream hemisphere wake, and changing the spacing between the two hemispheres means changing the location of the encroached area. When the spacing is small, streamline reattachment is disrupted, and the rough elements of the two hemispheres approach to form a single blunt rough element. When the spacing is in the medium transition region, the shear layer and vortex structure shed from the upstream hemisphere cross the upper part of the downstream hemisphere, and the disturbance effect is strongest in the normal direction. When the spacing is large, the streamlines have completed reattachment, and the interaction between the two hemispheres is weakest.

ACKNOWLEDGEMENTS

This work was supported by the National Natural Science Foundation of China [grant numbers 11602077, 11572357] and Natural Science Foundation of Hebei Province [grant number A2021202009].

CONFLICT OF INTEREST

No potential conflict of interest was reported by the authors.

AUTHOR CONTRIBUTIONS

P. Chen, J. Sun, W. Y. Chen contributed to the conception of the study; P. Chen, Y. T. Cheng performed the experiment; P. Chen, J. Sun, Y. T. Cheng contributed significantly to analysis and manuscript preparation; P. Chen performed the data analyses and wrote the manuscript; P. Chen, J. Sun, Y. T. Cheng, W. Y. Chen helped perform the analysis with constructive discussions.

REFERENCES

Acarlar, M. S., & Smith, C. R. (1987). A study of hairpin vortices in a laminar boundary layer. Part 1. Hairpin vortices generated by a hemisphere protuberance. *Journal of Fluid Mechanics*, 175, 1-41. https://doi.org/10.1017/S0022112087000272

Barman, K., Debnath, K., & Mazumder, B. S. (2016). Turbulence between two inline hemispherical obstacles under wave-current interactions. *Advances in Water Resources*, 88, 32-52. https://doi.org/10.1016/j.advwatres.2015.12.001

Cao, Y., & Tamura, T. (2020). Large-eddy simulation study of Reynolds number effects on the flow around a wall-mounted hemisphere in a boundary layer. *Physics of Fluids*, 32(2), 025109. https://doi.org/10.1063/1.5142371

Carr, I. A., & Plesniak, M. W. (2016). Three-dimensional flow separation over a surface-mounted hemisphere in pulsatile flow. *Experiments in Fluids*, 57(1), 9. https://doi.org/10.1007/s00348-015-2099-z

Citro, V., Luchini, P., Giannetti, F., & Auteri, F. (2015). Boundary-layer flows past an hemispherical roughness element: DNS, global stability and sensitivity analysis. *Procedia IUTAM*, 14, 173-181. https://doi.org/10.1063/1.4928533

Dai, R., Wei, A. Y., Luo, K., & Fan, J. R. (2012). Effects of two hemisphere roughness elements in turbulent boundary layer. *Journal of Engineering Thermophysics*, 33(12), 2104-2107.

Deng, S. C., Pan, C., Wang, J. J., & He, G. S. (2018). On the spatial organization of hairpin packets in a turbulent boundary layer at low-to-moderate Reynolds number. *Journal of Fluid Mechanics*, 844, 635. https://doi.org/10.1017/jfm.2018.160

Dong, S., Huang, Y., Yuan, X., & Lozano-Durán, A. (2020). The coherent structure of the kinetic energy transfer in shear turbulence. *Journal of Fluid Mechanics*, 892. https://doi.org/10.1017/jfm.2020.195

Gao, T. D., Sun, J., Chen, W. Y., Fan, Y., & Zhang, Y. T. (2021). Experimental investigation on the effect of particles on large scale vortices of an isolated hemispherical roughness element. *Physics of Fluids*, 33(6), 063308. https://doi.org/10.1063/5.0050773

Hamed, A. M., Peterlein, A. M., & Randle, L. V. (2019). Turbulent boundary layer perturbation by two wall-mounted cylindrical roughness elements arranged in tandem: Effects of spacing and height ratio. *Physics of Fluids*, 31(6), 065110. https://doi.org/10.1063/1.5099493

Jacobs, W. (1938). Flow behind a single roughness element. *Ingenieur-Archiv*, 7(36), 343-355.

Kim, T., Blois, G., Best, J. L., & Christensen, K. T. (2019). PIV measurements of turbulent flow overlying large, cubic- and hexagonally-packed hemisphere arrays. *Journal of Hydraulic Research*, 1-21. https://doi.org/10.1080/00221686.2019.1581671

Kim, T., & Christensen, K. T. (2018). Flow interactions between streamwise-aligned tandem cylinders in turbulent channel flow. *AIAA Journal*, 56(4), 1421-1433. https://doi.org/10.2514/1.j056186

Klebanoff, P., Tidstrom, K., & Sargent L. M. (1962). The Three-Dimensional Nature of Boundary-Layer Instability. *Journal of Fluid Mechanics*, 12, 1-34. https://doi.org/10.1017/S0022112062000014

Le, G. P., Chauve, M. P., Lima, R., & Rezende, J. (1990). Coupled wakes behind two circular cylinders. *Physical Review A*, 41(8), 4566. https://doi.org/10.1103/physreva.41.4566

Liu, J., Zou, L., Tao, F., Zuo, H. C., & Xu, H. B. (2022). Large eddy simulation of flow past two conical cylinders in tandem arrangement. *Chinese Journal of*

Theoretical and Applied Mechanics, 54(5), 1-11. https://doi.org/10.6052/0459-1879-21-653

Lumley, J. L. (1967). The structure of inhomogeneous turbulent flows. *Atmospheric Turbulence and Radio Wave Propagation*, 166–178.

Mochizuki, M. (1961). Smoke observation on boundary layer transition caused by a spherical roughness element. *Journal of the Physical Society of Japan*, 16(5), 995-1008. https://doi.org/10.1143/jpsj.16.995

Noack, B. R. (2016). From snapshots to modal expansions-bridging low residuals and pure frequencies. *Journal of Fluid Mechanics*, 802, 1-4. https://doi.org/10.1017/jfm.2016.416

Savory, E., & Toy, N. (1986). Hemispheres and hemisphere-cylinders in turbulent boundary layers. *Journal of Wind Engineering and Industrial Aerodynamics*, 23, 345-364. https://doi.org/10.1016/0167-6105(86)90054-1

Savory, E., & Toy, N. (1988). The separated shear layers associated with hemispherical bodies in turbulent boundary layers. *Journal of Wind Engineering and Industrial Aerodynamics*, 28, 291-300. https://doi.org/10.1016/0167-6105(88)90125-0

Sirovich, L. (1987). Turbulence and the dynamics of coherent structures. I. Coherent structures. *Quarterly of Applied Mathematics*, 45(3), 561-571. https://doi.org/10.1090/qam/910464

Spivack, H. M. (1946). Vortex frequency and flow pattern in the wake of two parallel cylinders at varied spacing normal to an air stream. *Journal of the Aeronautical Sciences*, 13(6): 289-301. https://doi.org/10.2514/8.11375

Sumner, D., Wong, S. S. T., Price, S. J., & Paidoussis, M. P. (1999). Fluid behaviour of side-by-side circular cylinders in steady cross-flow. *Journal of Fluids & Structures*, 13(3), 309-338. https://doi.org/10.1006/jfls.1999.0205

Waigh, D. R., & Kind, R. J. (1998). Improved aerodynamic characterization of regular three-dimensional roughness. *AIAA Journal*, 36(6), 1117-1119. https://doi.org/10.2514/2.491

Wassermann, P., & Kloker, M. (2002). Mechanisms and passive control of crossflow-vortex-induced transition in a three-dimensional boundary layer. *Journal of Fluid Mechanics*, 456, 49-84. https://doi.org/10.1017/s0022112001007418

Wu, S., Christensen, K. T., & Pantano, C. (2020). A study of wall shear stress in turbulent channel flow with hemispherical roughness. *Journal of Fluid Mechanics*, 885. https://doi.org/10.1017/jfm.2019.968

Xu, G., & Zhou, Y. (2004). Strouhal numbers in the wake of two inline cylinders. *Experiments in Fluids*, 37, 248–256. https://doi.org/10.1007/s00348-004-0808-0

Yan, D., Sun, J., Gao, T. D., Chen, P., Cheng, Y. T., & Chen, W. Y. (2021). Experimental study on the effect of solid particles on riblet-plate turbulent boundary layer. *Chinese Journal of Theoretical and Applied Mechanics*, 53(8), 2279-2288. https://doi.org/10.6052/0459-1879-21-149

Zdravkovich, M. M. (1987). The effects of interference between circular cylinders in cross flow. *Journal of Fluids and Structures*, 1(2), 239-261. https://doi.org/10.1016/s0889-9746(87)90355-0

Zhang, K., Ma, C., Zhang, J., Zhang, B., & Zhao, B. (2021). Drag reduction characteristics of bionic structure composed of grooves and mucous membrane acting on turbulent boundary layer. *Journal of Applied Fluid Mechanics*, 15(1), 283-292. https://doi.org/10.47176/JAFM.15.01.32901

Zhang, Y. T., Sun, J., Gao, T. D., & Fan, Y. (2020). Experimental study of the effect of solid particles on hemispheric disturbance wake. *Chinese Journal of Theoretical and Applied Mechanics*. 52(03), 728-739. https://doi.org/10.6052/0459-1879-19-353

Zhou, Y., & Yiu, M. W. (2006). Flow structure, momentum and heat transport in a two-tandem-cylinder wake. *Journal of Fluid Mechanics*, 548(-1), 17-48. https://doi.org/10.1017/s002211200500738x